# Supporting Information

Efficient and Selective Photocatalytic $CO_2$ Conversion Enabled by FePc Nanosheets in a Dye-Sensitized System

Hua Gao, [a] Yong Zhu, [a] Zhibing Wen, [a] Ran Zhao, [a] Zhi Chen, [a] Siyao Wang, [a] Shuanglin He, [a] Kuang Peng, [a] Yiwen Tang, [a] Licheng Sun, [a,b] Fei Li* [a]

[a] State Key Laboratory of Fine Chemicals, Frontier Science Center for Smart Material, Dalian University of Technology, Dalian 116024, China.

[b] Center of Artificial Photosynthesis for Solar Fuels, School of Science, Westlake University, Hangzhou 310024, China.

Corresponding Author: Prof. F. Li* E-mail: lifei@dlut.edu.cn

## 1. Time-Resolved Fluorescence Spectroscopy (TRFS)

### Part I: Sample Preparation and Deoxygenation

A small amount of the powder was accurately weighed and dispersed in spectrophotometric-grade or HPLC-grade N, N-Dimethylformamide (DMF) to prevent interference from fluorescent impurities. The suspension was subjected to ultrasonication for 10-30 minutes to effectively break up particle agglomerations and form a relatively stable, homogeneous suspension. The well-dispersed suspension was then transferred into a quartz cuvette with four transparent windows, leaving sufficient headspace. A slender argon gas tube was inserted into the bottom of the suspension. Deoxygenation was performed by purging with high-purity argon (99.999%) at a slow, steady flow rate for 15-25 minutes.

### Part II: Instrument Setup and Measurement

The FLS1000 spectrophotometer system was initialized by sequentially turning on the main unit, the pulsed laser for time-correlated single photon counting (TCSPC), and the detector, followed by launching the Fluoracle software for initialization. A pulsed laser diode with an excitation wavelength of 450 nm was selected, and an appropriate repetition rate was set. The prepared sample was placed in the sample chamber, and data acquisition was initiated. The count rate was monitored in real-time to ensure it

remained stable and below 1-2% of the laser's repetition rate to avoid pulse pile-up distortion. An acquisition target was set, such as reaching 100000 counts in the peak channel or a total acquisition time of 10 minutes, to ensure an adequate signal-to-noise ratio.

**Part III: Data Acquisition and Analysis**

With the deoxygenated sample in place, data collection was started while continuously monitoring the stability of the count rate. In the fitting module of the software, the recorded decay curve was loaded and fitted using a tri-exponential model. Finally, the normalized data were compared to analyze the fluorescence lifetimes

## 2. Transient Absorption Spectroscopy (TAS)

The transient absorption kinetics were investigated using an Edinburgh Instruments LP980-KA spectrometer operating in kinetic mode. The powdered sample was dispersed in spectroscopic-grade dimethylformamide (DMF) via ultrasonication to form a homogeneous suspension. This suspension was then loaded into a standard quartz cuvette, selected specifically to facilitate the essential orthogonal pump-probe beam geometry for highly scattering samples. The sample was photoexcited at 355 nm using the third harmonic output of a Nd:YAG nanosecond laser (Spectra-Physics, Quanta-Ray LAB-130-10) operating at a 10 Hz repetition rate, with a typical fluence of 0.5 mJ $cm^{-2}$. Prior to data acquisition, the suspension was purged with high-purity carbon dioxide for 15 minutes to quench interfering signals from molecular oxygen. This purging was continued throughout the measurement to maintain an oxygen-free environment. The transient decay profiles were recorded at a fixed probe wavelength by averaging the signals over 256 laser pulses using a fast silicon photodiode detector. The obtained transient decay kinetics were analyzed by fitting to a tri-exponential function. The model is expressed as:

$$\Delta A(t) = A_1 \exp(-t/\tau_1) + A_2 \exp(-t/\tau_2) + A_3 \exp(-t/\tau_3)$$

where $\Delta A(t)$ is the transient absorption signal amplitude at time *t*, $A_i$ are the pre-exponential factors (amplitude) corresponding to each kinetic phase, and $\tau_i$ are the

characteristic lifetimes of the respective processes. The quality of the fit was assessed by the reduced chi-squared value ($\chi^2$) and the randomness of the residuals.

### 3. In-situ Attenuated Total Reflectance Infrared (ATR-IR) Spectroscopy

In situ ATR-IR spectroscopy was conducted using a Nicolet iS50 FT-IR spectrometer equipped with a dedicated in situ ATR accessory to monitor the reaction intermediates and adsorbed species on the catalyst surface during the photocatalytic $CO_2$ reduction process in real time. The catalyst film was prepared as follows: 5 mg of catalyst powder was dispersed in a mixture of 600 μL ethanol, 400 μL ultrapure water, and 30 μL Nafion solution, followed by ultrasonication to form a homogeneous slurry. The resulting slurry was drop-cast onto a meticulously cleaned silicon ATR crystal and dried at room temperature to form a uniform catalyst-loaded film. The catalyst-coated crystal was then assembled into the reaction cell, followed by the introduction of a DMF solution containing BIH (as a sacrificial agent). A continuous flow of $CO_2$ was maintained to allow the reactants to reach adsorption equilibrium on the catalyst surface. A single-beam spectrum collected under these conditions was used as the background reference. The reaction was initiated by irradiating the sample with a 450nm LED light source. Utilizing the time-resolved acquisition function of the Nicolet iS50 spectrometer, infrared spectra were automatically collected at predetermined time intervals during the reaction to track the dynamic evolution of surface species in real time.

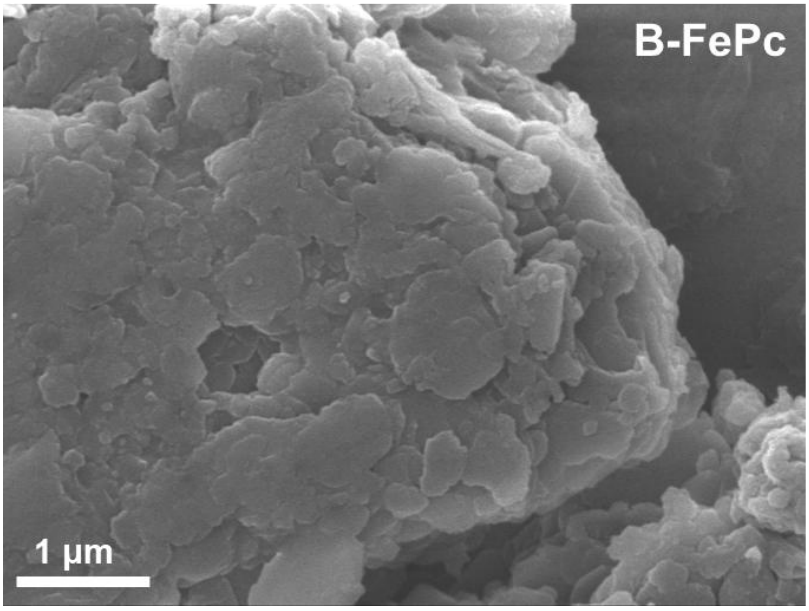


Figure S1. SEM image of B-FePc.

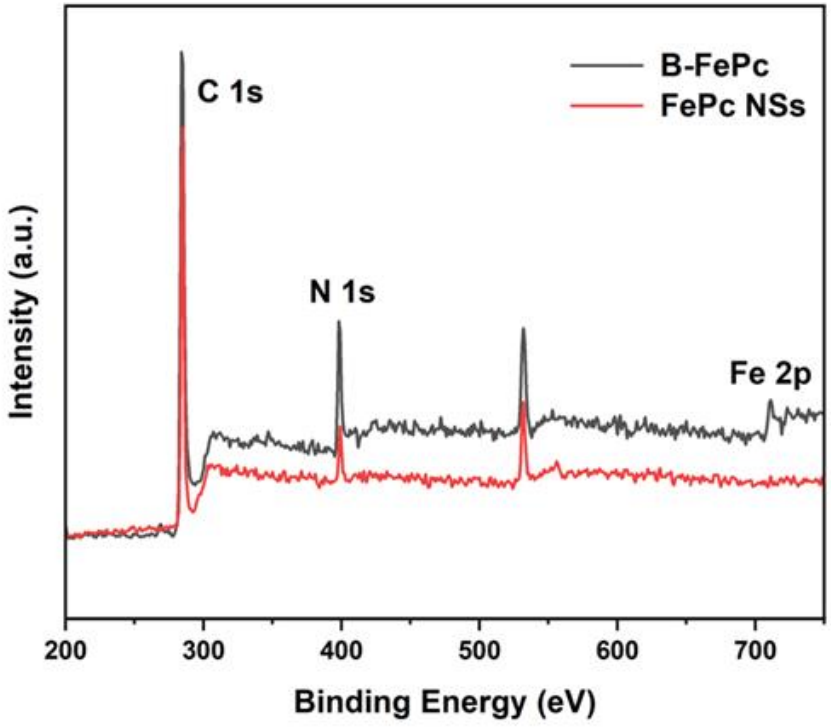


Figure S2. XPS survey spectra of B-FePc and 2D FePc NSs.


Figure S3. Optical photograph of high-yield of FePc NSs suspension.

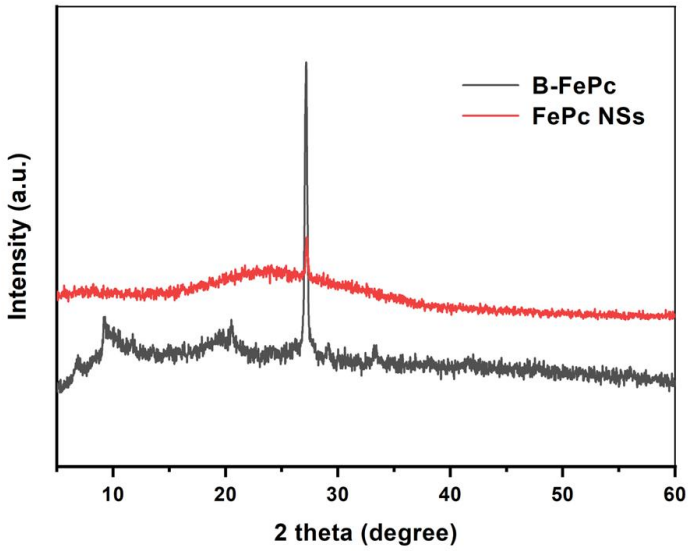


Figure S4. XRD patterns of B-FePc and 2D FePc NSs.

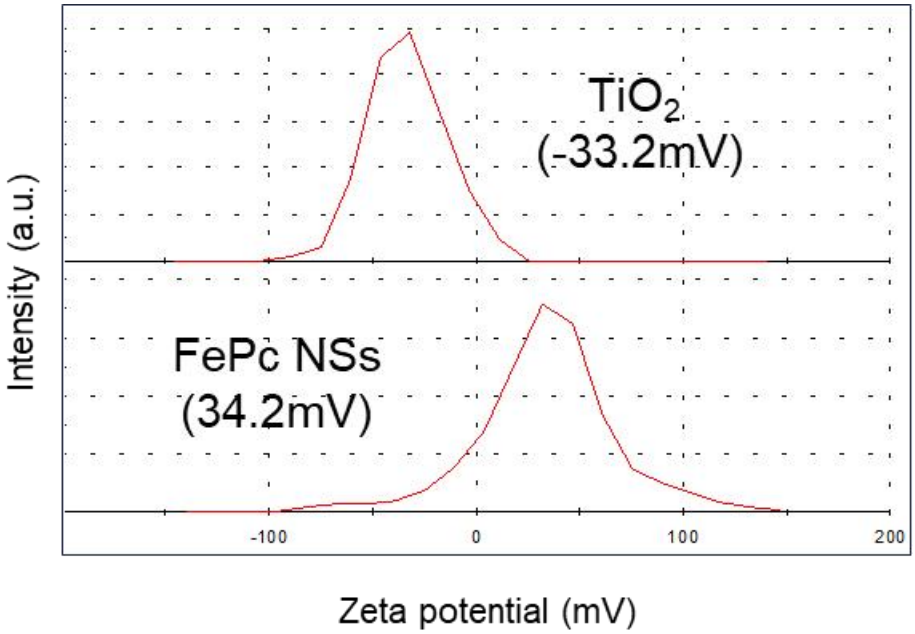


Figure S5. Zeta potential determination of $TiO_2$ and FePc NSs in ethanol solution.

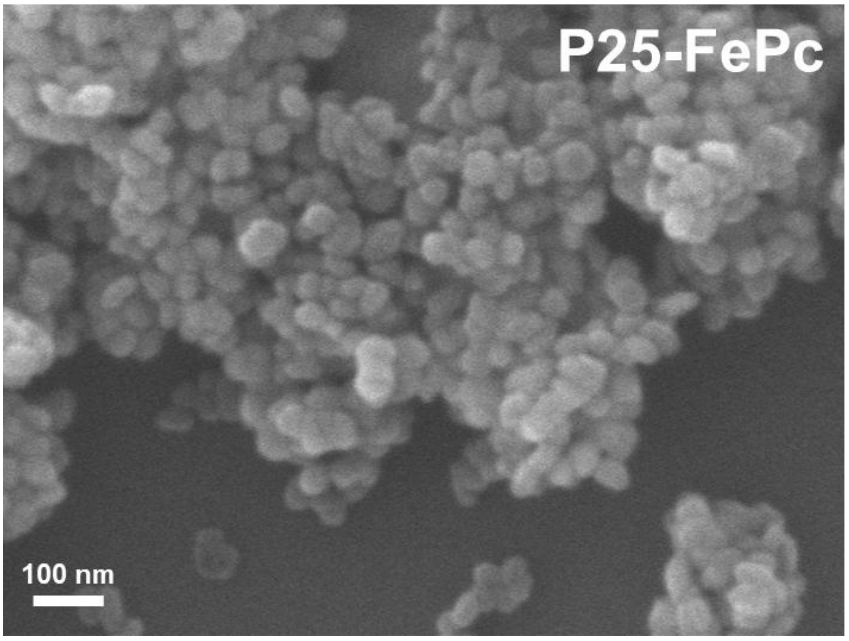


Figure S6. SEM of $TiO_2$-FePc NSs.

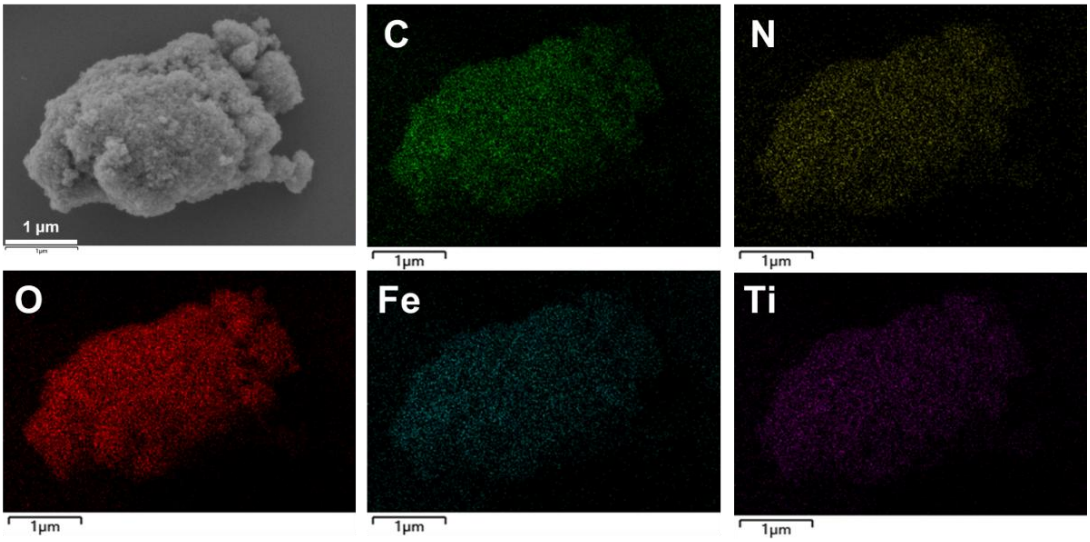


Figure S7. SEM and the corresponding EDS mapping of $TiO_2$-FePc NSs.

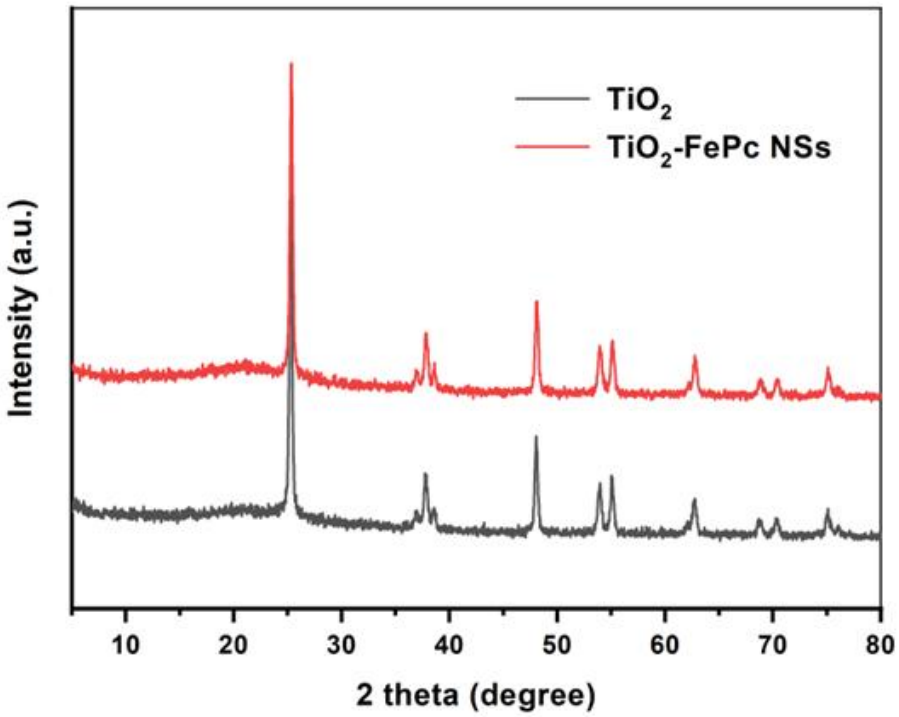


Figure S8. XRD patterns of $TiO_2$ and $TiO_2$-FePc NSs.

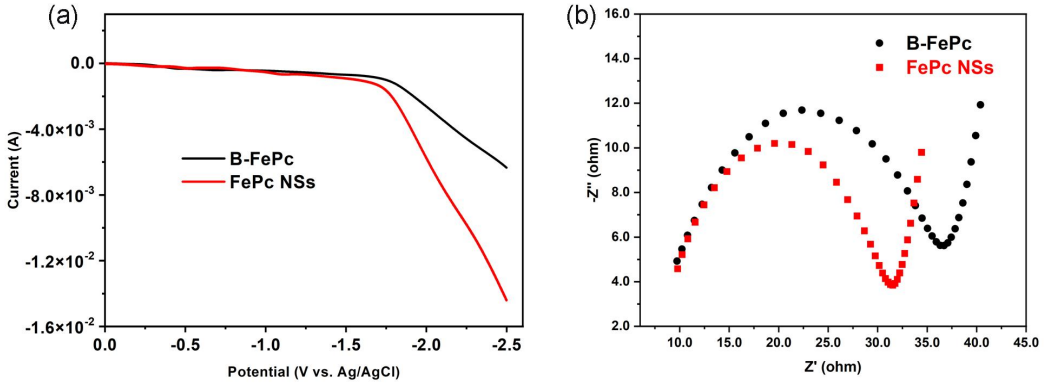


Figure S9. (a) Linear sweep voltammetry curves, and (b)EIS Nyquist plots of B-FePc and 2D FePc NSs.

Figure S10. Photocatalytic equipment used for photocatalytic carbon dioxide reduction.

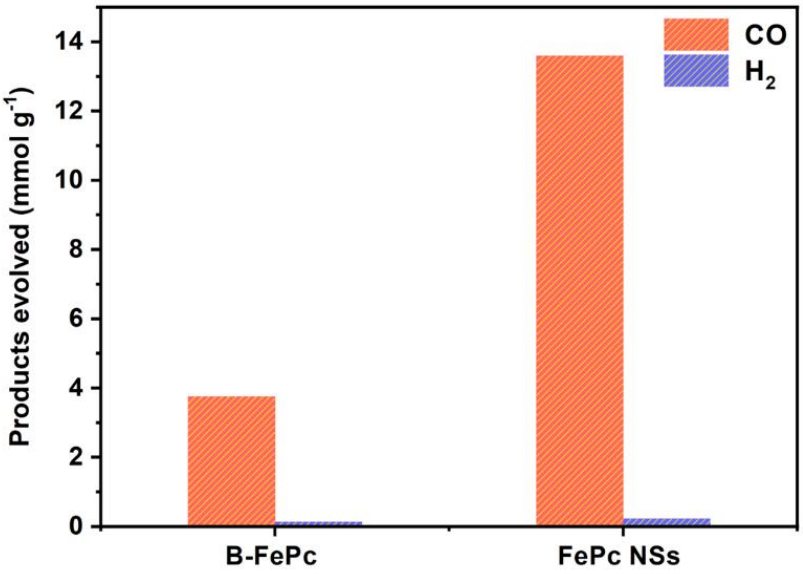


Figure S11. Photocatalytic $CO_2$ reduction performance under illumination ($\lambda_{LED}$ = 450 nm, 0.2mg $[Ru(bpy)_3]Cl_2 \cdot 6H_2O$, 25 mM BIH, 0.1 M phenol, 10h) with 0.2mg B-FePc or 2D FePc NSs.

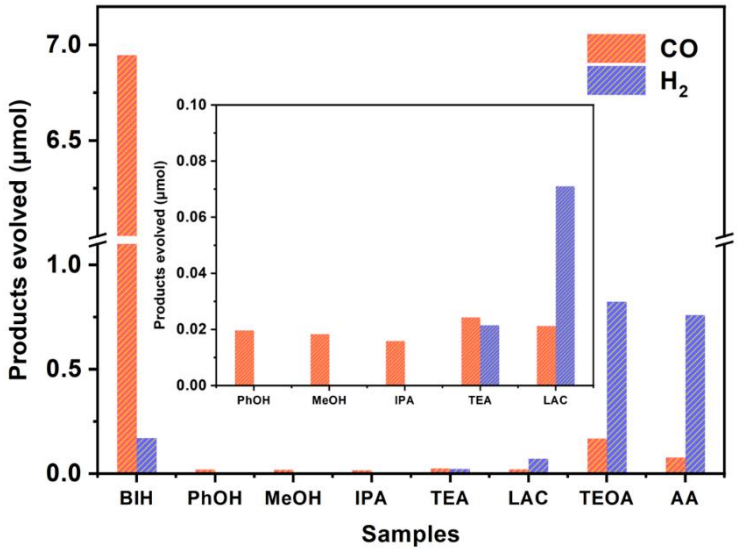


Figure S12. Photocatalytic $CO_2$ reduction performance of RuP-$TiO_2$-FePc NSs (1 wt%) under illumination ($\lambda_{LED}$ = 450 nm, 5 mg samples, 10h) with different electron donors (0.1 M).

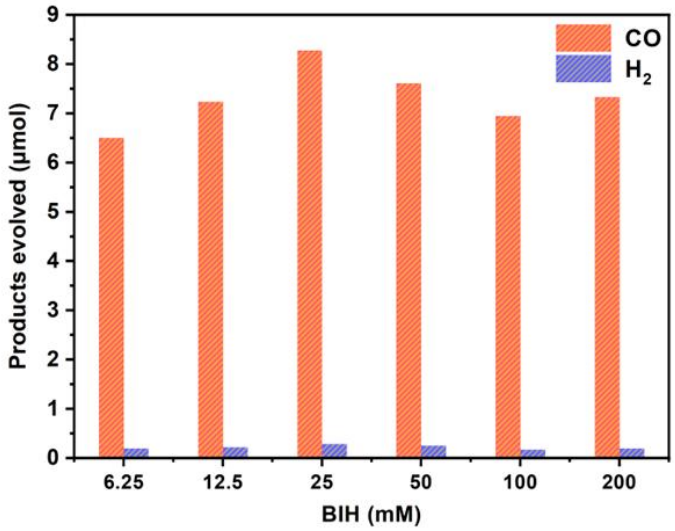


Figure S13. Photocatalytic $CO_2$ reduction performance of RuP-$TiO_2$-FePc NSs (1 wt%) under illumination ($\lambda_{LED}$ = 450 nm, 5 mg samples, 10h) with different BIH concentrations .

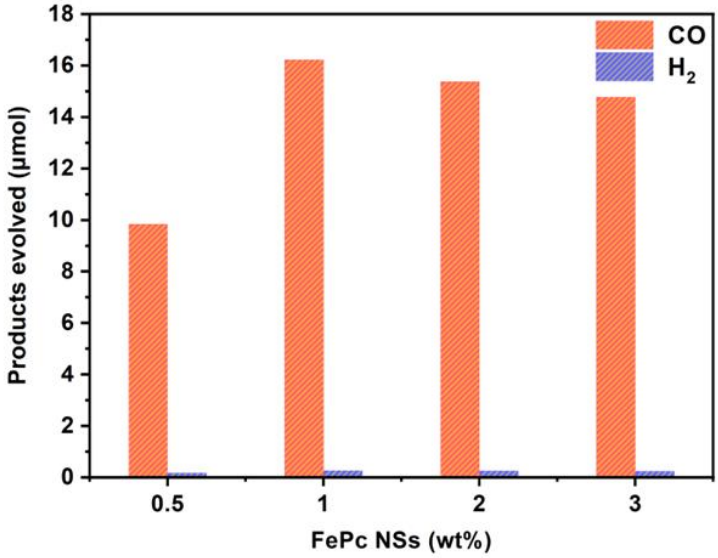


Figure S14. Photocatalytic $CO_2$ reduction performance of RuP-$TiO_2$-FePc NSs under illumination ($\lambda_{LED}$ = 450 nm, 5 mg samples, 25 mM BIH, 0.1 M phenol, 10h) with different FePc NSs contents. NOTE: The variation in FePc loading simultaneously modulates the surface RuP-to-FePc NSs molar ratio under the saturated dye adsorption conditions, with the optimal performance at 1 wt% corresponding to the most efficient sensitizer/catalyst stoichiometry.

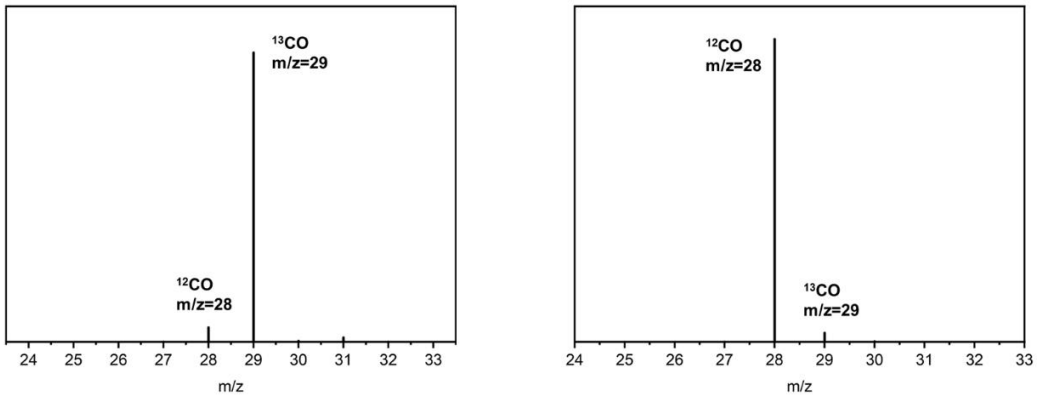


Figure S15. Mass spectra of gas products ($^{12}$CO, m/z = 28 and $^{13}$CO, m/z = 29) after 10 h of photocatalysis.

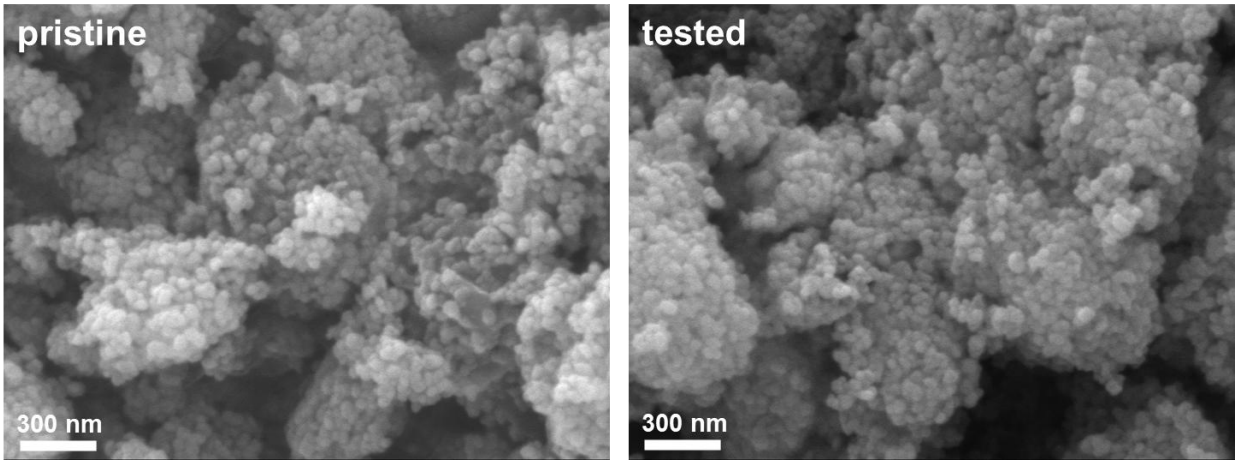


Figure S16. SEM images of (a) pristine, and (b) tested RuP-$TiO_2$-FePc NSs after 40h of illumination .

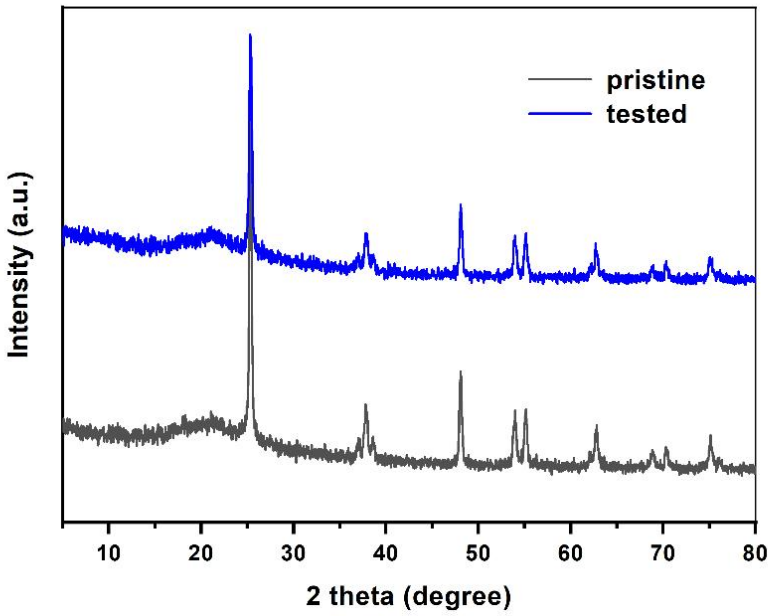


Figure S17. XRD patterns of the pristine and tested RuP-$TiO_2$-FePc NSs after 40h of illumination .

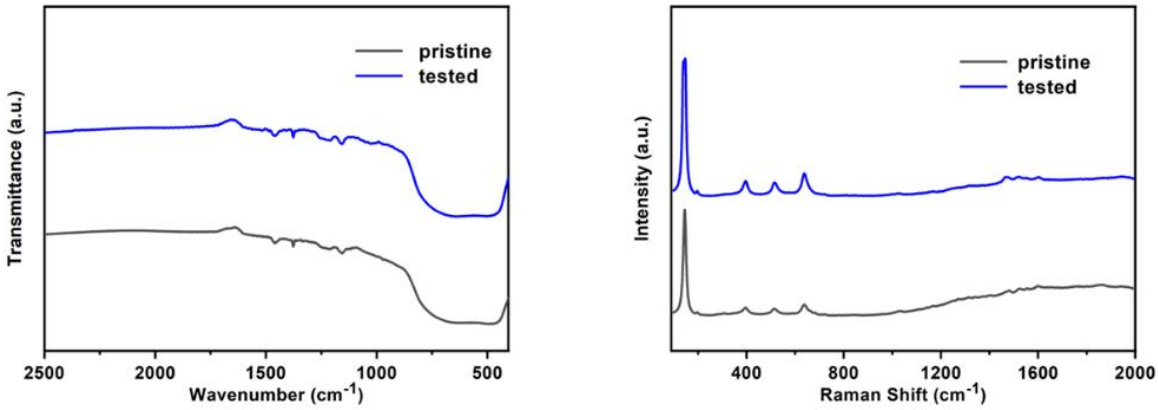


Figure S18. (a) FT-IR spectra, and (b) Raman spectra of the pristine and tested RuP-$TiO_2$-FePc NSs after 40h of illumination .

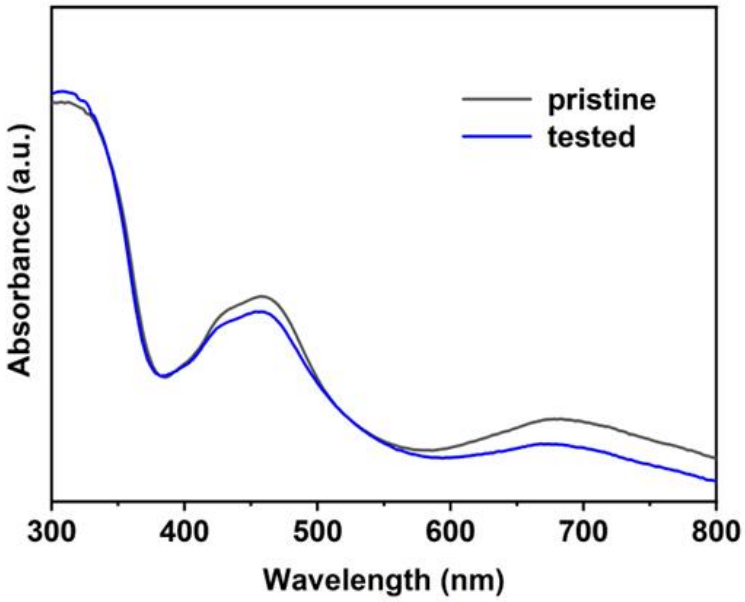


Figure S19. UV-Vis spectra of the pristine and tested RuP-$TiO_2$-FePc NSs after 40h of illumination .

Table S1. FePc NSs content in ethanol solution and RuP content in RuP-$TiO_2$-FePc NSs (1 wt%), obtained from the ICP-OES

| Samples | contents |
|---|---|
| FePc NSs | 24 μg FePc /ml (ethanol) |
| RuP-$TiO_2$-FePc NSs (1 wt%) | 5 μg RuP/mg (cat) |

Table S2. Results of photocatalytic $CO_2$ reduction under various conditions after 10 h of illumination (450 nm, 25 mM BIH, 10 ml DMF ).

| Entry | NPs | $H^+$ | CO[a] | $H_2$[a] | selectivity[b] |
|---|---|---|---|---|---|
| 1 | RuP-$TiO_2$-FePc NSs (1 wt%) | phenol[j] | 16.23 | 0.27 | 98.36 |
| 2 | RuP-$TiO_2$-FePc NSs (1 wt%) | - | 8.28 | 0.29 | 96.62 |
| 3[c] | RuP-$TiO_2$-FePc NSs (1 wt%) | phenol | ND[d] | ND | ND |
| 4[e] | RuP-$TiO_2$-FePc NSs (1 wt%) | phenol | ND | ND | ND |
| 5[f] | RuP-$TiO_2$-FePc NSs (1 wt%) | phenol | ND | 0.1 | ND |
| 6[g] | $TiO_2$-FePc NSs (1 wt%) | phenol | 0.03 | 0.02 | 60 |
| 7[h] | RuP-$TiO_2$ | phenol | 0.88 | 0.03 | 96.7 |
| 8[i] | RuP + FePc NSs | phenol | 0.84 | 0.02 | 97.67 |
| 9 | RuP-$Al_2O_3$-FePc NSs (1 wt%) | phenol | 5.34 | 0.7 | 88.41 |
| 10 | RuP-$TiO_2$-FePc NSs (1 wt%) | Phenol-d6[k] | 9.32 | 0.06 | 99.34 |

[a] CO and $H_2$ quantities in μmol. [b] Selectivity of CO, %. [c] Without light irradiation. [d] ND:Not detected. [e] Without BIH. [f] Without $CO_2$. [g] Without RuP. [h] Without FePc NSs. [i] Without $TiO_2$. [j] 0.1 M. [k] 0.1 M

Table S3. Comparison of the performance of $TiO_2$-based photocatalysts for $CO_2$ reduction reported in the recent literatures (dye-sensitized photocatalytic systems).

| Entry | PS | Cat. | Rate[a] | TOF($h^{-1}$) [b] | selectivity[c] | TON[d] | light[e] | Ref. |
|---|---|---|---|---|---|---|---|---|
| 1 | ZnP/BDP | CoQPy | 25.27 (40h) | 18.98 (40h) | 66% | 759 | [1] | 1 |
| 2 | N719/ZnP | Fe(o-TMA) | ~18 (40h) | 16.2 (40h) | >99% | 1658 | [1] | 2 |
| 3 | $ZnP_{CNPA}$ | ReC | 27.76 (56h) | 18.04 (56h) | - | 1015 | [2] | 3 |
| 4 | D-A dye | ReC | 18.7 (20h) | 12.16 (20h) | ~73% | ~244 | -- | 4 |
| 5 | D-A dye | ReC | 29.1 (30h) | 18.92 (30h) | - | 570 | -- | 5 |
| 6 | D-A dye | ReC | 18.38 (10h) | 11.95 (10h) | - | 435 | -- | 6 |
| 7 | IrP | ReC | 10.42 (41h) | 6.77 (41h) | >99% | 730 | -- | 7 |
| 8 | D-A dye | Re-H | 28.95 (32h) | 18.00 (32h) | 97% | 922 | -- | 8 |
| 9 | HO-TPA | ReP | 32.86 (26h) | 21.36 (26h) | - | 534 | -- | 9 |
| 10 | RuP | FePc NSs | 27.3 (40h) | 15.52 (40h) | >98% | 1363 | [3] | This work |

**[a]** CO production rates are reported in the unit of mmol $g^{-1}_{(active\ catalyst)}$ $h^{-1}$, where "active catalyst" refers to the mass of the catalytic metal-complex or molecular active site (e.g., CoQPy, Fe(o-TMA), ReC, FePc, etc.) as specified in each corresponding publication. For the present work, the rate is 27.3 mmol $g^{-1}_{(FePc)}$ $h^{-1}$, calculated based on the mass of the FePc NSs active component. For reference, the rate normalized to the total mass of the RuP-$TiO_2$-FePc NSs composite (1 wt% FePc NSs) is 0.273 mmol $g^{-1}_{(composite)}$ $h^{-1}$.

**[b]** Turnover frequency (TOF) calculated as moles of CO produced per mole of active catalyst per hour. Note that entries [a] and [b] both quantify CO production rates, where [a] represents mass activity and [b] represents intrinsic (turnover) activity. The divergence in their numerical values arises from the distinct molecular weights of the catalytic centers.

**[c]** Selectivity towards CO in the gas-phase products ($H_2$ as main by-product).

**[d]** All $TON_{(CO)}$ values were calculated based on the molar amount of the respective active catalyst component. The literature data were either taken directly from the reported values or calculated based on the information provided in the original

publications.

**[e]** Light intensity (mW/cm$^2$) and wavelength for each entry are provided in footnotes [1]–[3] below; "--" indicates data not explicitly reported in the original publication. [1] LED irradiation at 525 nm (10 mW/cm$^2$) or 450 nm (34 mW/cm$^2$) or 6200 K cold white light (29 mW/cm$^2$). [2] the actual intensities of irradiated light were determined as follows: 109, 207, and 414 mW/cm$^2$. [3] 450 nm LED (130 mW/cm$^2$).

Table S4. Tri-exponential decay time constants of time-resolved photoluminescence for different samples.

| Sample | $A_1$ | $\tau_1$/ns | $A_2$ | $\tau_2$/ns | $A_3$ | $\tau_3$/ns | $\tau_{int}$/ns |
|---|---|---|---|---|---|---|---|
| 1 | 2563.74 | 108.62 | 10625.59 | 303.39 | 2216.64 | 506.03 | 340.82 |
| 2 | 6749.45 | 67.23 | 14298.13 | 227.34 | 2126.80 | 445.50 | 256.16 |
| 3 | 21056.22 | 37.47 | 23614.48 | 136.02 | 2565.76 | 331.90 | 154.37 |
| 4 | 17755.04 | 50.38 | 10037.35 | 144.60 | 1467.62 | 394.82 | 165.35 |
| 5 | 11453.59 | 66.58 | 19205.07 | 204.66 | 1966.20 | 438.07 | 221.90 |

1. RuP-$Al_2O_3$, 2. RuP-$TiO_2$, 3. RuP-$TiO_2$-FePc NSs, 4. RuP-$TiO_2$-FePc NSs + BIH, 5. RuP-$Al_2O_3$-FePc NSs.

The photoluminescence (PL) decay kinetics were analyzed by fitting the time-resolved photoluminescence (TR-PL) spectra with a tri-exponential decay function of the form $I(t)=I_0+A_1\exp(-t/\tau_1)+A_2\exp(-t/\tau_2)+A_3\exp(-t/\tau_3)$, where $A_i$ and $\tau_i$ represent the relative amplitude and the decay time of the i-th component, respectively. To provide a singular, representative metric of the emission lifetime, the amplitude-weighted average lifetime ($\tau$), was calculated using the standard equation: $\tau = \sum A_i\tau_i^2 / \sum A_i\tau_i$ . This method of averaging is appropriate as it weights each lifetime component by its contribution to the total steady-state emission intensity, thereby yielding a value that is directly correlated with the sample's overall quantum yield and providing a more accurate representation of the composite excited-state dynamics.

Table S5. Transient absorption kinetics fitted to a triexponential function.

| Sample | $A_1$ | $\tau_1$/ns | $A_2$ | $\tau_2$/ns | $A_3$ | $\tau_3$/ns | $\tau_{ave}$/ns |
|---|---|---|---|---|---|---|---|
| 1 | 0.027 | 9.963 | 0.016 | 103.6 | 0.014 | 1158 | 1044.62 |
| 2 | 0.018 | 6.381 | 0.017 | 34.45 | 0.008 | 94.92 | 63.70 |

**1. RuP-$TiO_2$-FePc NSs, 2. RuP-$TiO_2$-FePc NSs + BIH**

Reference


[1] V. Nikolaou, C. Govind, E. Balanikas, J. Bharti, S. Diring, E. Vauthey, M. Robert, F. Odobel, *Angew. Chem. Int. Ed.,* **2024**, 63, e202318299.

[2] V. Nikolaou, P.B. Pati, H. Terrisse, M. Robert, F. Odobel, *EES Catal.,* **2024**, 2, 1314-1319.

[3] D.-I. Won, J.-S. Lee, Q. Ba, Y.-J. Cho, H.-Y. Cheong, S. Choi, C.H. Kim, H.-J. Son, C. Pac, S.O. Kang, *ACS Catal.,* **2018**, 8, 1018-1030.

[4] J.S. Lee, D.I. Won, W.J. Jung, H.J. Son, C. Pac, S.O. Kang, *Angew. Chem. Int. Ed.,* **2016**, 56, 976-980.

[5] D.-I. Won, J.-S. Lee, J.-M. Ji, W.-J. Jung, H.-J. Son, C. Pac, S.O. Kang, *J. Am. Chem. Soc.,* **2015**, 137, 13679-13690.

[6] E.-G. Ha, J.-A. Chang, S.-M. Byun, C. Pac, D.-M. Jang, J. Park, S.O. Kang, *Chem. Commun.,* **2014**, 50, 4462-4464.

[7] P.S. Kim, S. Choi, S.Y. Kim, J.H. Jo, Y.S. Lee, B. Kim, W. Kim, W. Choi, C.H. Kim, H.J. Son, C. Pac, S.O. Kang, *Chem. Eur. J.,* **2019**, 25, 13609-13623.

[8] S. Choi, Y.-J. Kim, S. Kim, H.S. Lee, J.Y. Shin, C.H. Kim, H.-J. Son, S.O. Kang, *ACS Appl. Energy Mater.,* **2022**, 5, 10526-10541.

[9] Y.-F. Chen, J.-F. Huang, M.-H. Shen, J.-M. Liu, L.-B. Huang, Y.-H. Zhong, S. Qin, J. Guo, C.-Y. Su, *J. Mater. Chem. A,* **2019**, 7, 19852-19861.